

Microstructure of viscoelastic thermal compressed (VTC) wood using computed microtomography

Gernot Standfest*, Andreja Kutnar, Bernhard Plank, Alexander Petutschnigg, Frederick A. Kamke, Manfred Dunky

Gernot Standfest (corresponding author)

Forest Products Technology and Timber Constructions, Salzburg University of Applied Sciences, Markt 136a, Kuchl 5431, Salzburg, Austria

+43(0)50-2211-2406

+43(0)50-2211-2099

gernot.standfest@fh-salzburg.ac.at

www.fh-salzburg.ac.at

Andreja Kutnar

Andrej Marusic Institute, University of Primorska, 6000 Koper, Slovenia, ILTRA d.o.o., Celovska cesta 268, 1000 Ljubljana, Slovenia

Bernhard Plank

Research Group Computed Tomography, Upper Austrian University of Applied Sciences, Stelzhamerstraße 23, Wels 4600, Upper Austria, Austria

Alexander Petutschnigg

Forest Products Technology and Timber Constructions, Salzburg University of Applied Sciences, Markt 136a, Kuchl 5431, Salzburg, Austria

Frederick A. Kamke

Department of Wood Science and Engineering, Oregon State University, 119 Richardson Hall, Corvallis, Oregon 9733, USA

Manfred Dunky

University of Natural Resources and Life Sciences, Peter Jordan Strasse 82, 1190 Vienna, Austria

Abstract

The paper describes for the first time the analysis of the structure of compressed wood using computed tomography. The anatomical structures of Douglas-fir and hybrid poplar before and after densification with the Viscoelastic Thermal Compression (VTC) process were described by pore size distributions and mean pore sizes and compared. The compression of Douglas-fir mainly affected earlywood, while the compression of hybrid poplar mainly occurred in the vessels. In both wood species the densification resulted in a significant decrease in the pore volumes. The porosity decreased to less than the half of the original value for Douglas-fir earlywood

and to approximately one quarter for the vessels in hybrid poplar. The relevant mean pore sizes also decreased dramatically down to about one quarter compared to the original values. In contrast, latewood in Douglas-fir and libriform fibers in hybrid poplar are quite stable under compression. Douglas-fir latewood retained its original structure after compression and did not show any reduction in pore size.

The results confirmed that the anatomical structure of VTC densified wood can be described by pore size distributions and mean pore sizes. However, in the case of broad or bimodal distributions the mean pore sizes are of less significance.

Keywords

VTC wood; porosity; pore size distribution; granulometry; computed microtomography; image analysis

Introduction

The poor mechanical properties of low-density wood can be improved by wood densification (Seborg et al. 1945, Inoue et al. 1993, Dwianto et al. 1999, Navi and Girardet 2000, Blomberg and Persson 2004). Among other relevant technologies, the so-called Viscoelastic Thermal Compression (VTC) process densifies wood material by compression in transverse direction without cell wall fracture, yielding increased strength, stiffness, and hardness (Kamke and Sizemore 2008, Kutnar et al. 2008). The wood morphology changes significantly during the VTC process and depends strongly upon the degree of densification (Kutnar et al. 2009). Densification is achieved by high strain reducing the void space mainly of the cell lumen by cell wall buckling, but without destruction of the micro-cellular structure of the wood (Kutnar et al. 2009). The as yet undamaged cell walls, hence, are a major factor in the improved properties of VTC wood (Wolcott 1989, Kultikova 1999, Navi and Girardet 2000, Kamke and Sizemore 2008).

Tomographic imaging provides a powerful tool for investigating the microstructure of materials. Microfocus computed tomography (CT) demonstrated its suitability when investigating wooden tissues with resolutions of 300 μm down to 21 μm (Okochi et al. 2007, Grabner et al. 2009, Scholz et al. 2010). Most recent findings on the microstructure of wood based materials were derived using synchrotron radiation CT (Illman and Dowd 1999, Mannes et al. 2010, Modzel et al. 2011) with resolutions of around 7 μm down to nearly 1 μm , while synchrotron radiation-based phase contrast tomography even yields resolutions of 2 μm down to 0.7 μm (Trtik et al. 2007, Mayo et al. 2009, 2010, Derome et al. 2011). In the investigations reported in this paper, a tube based x-ray source was used for x-ray microtomography, with a resolution theoretically down to 0.4 μm .

Mercury intrusion porosimetry (MIP) enables determination of the porosity of wood when incrementally increasing pressures are applied. However, interpretation of the pore size distribution gained by MIP can be affected by the so-called “bottleneck-effect”; the high pressure necessary to make mercury flow through pit openings leads to results with a higher proportion of small pores with a diameter below 1 μm (Schneider and Wagner 1974; Pfriem et al. 2009, Scholz et al. 2010). Also high proportions of wood rays in hardwoods cause large errors in determination of the pore size distribution with MIP (Schneider 1979). Additionally cell wall cavities with small diameters are compressed (Pfriem et al. 2009). According to Scholz et al. (2010) it can be demonstrated by CT that not all pores are accessible by MIP. MIP was applied to measure the porosity of the surface layer of particleboards (Schneider 1982) and of single layer particleboards (Schweitzer and Niemz 1991).

The aim of this paper was (i) a methodological advancement when analyzing the microstructure of densified wood, determining absolute (total number of voxels belonging to a certain pore size) and relative pore size distributions (frequency of pore sizes) and (ii) an improved knowledge of the microstructure of densified wood, like the cell structure. A squeezed but still intact cell structure after densification improves the material performance; the thorough analysis of such densification behavior shall enable a further development of the VTC process. Up to now densified wood was rather classified according to its macroscopic behavior and performance than according to its microstructure in deformed state; CT investigations of densified wood have not yet been reported in scientific literature. In these investigations special emphasis was placed on the correct choice of sample size in order to guarantee accurate statistical representation of the results. This implies a compromise between the largest possible sample sizes, the volume of data to be processed, and the achievable resolution in the anatomical structure analysis.

Material and Methods

Materials for the VTC Process

Air dried low-density hybrid poplar (*Populus deltoides* × *Populus trichocarpa*) from a plantation located in northeastern Oregon and Douglas-fir (*Pseudotsuga menziesii*) were sawn and planed into 6 mm thick (radial) specimens and cut to a length and width of 100 mm (longitudinal) and 60 mm (tangential), respectively. The specimens were kept under specific climatic conditions (20°C, 65% relative humidity) until equilibrium moisture content of approx. 12 % was reached.

Compression Process

Transverse compression of wood in radial direction under transient conditions at 170° C was performed in a pressurized vessel equipped with a heated hydraulic press. Specimens were first exposed to saturated steam for 3 minutes at 170° C. The steam pressure of 773 kPa was released and 10 seconds later the compression stress was applied. Therefore, transient conditions of moisture content and temperature in the specimens were obtained before compression. A stress level of 5.5 MPa for both Douglas-fir and hybrid poplar was applied using a manually controlled hydraulic cylinder, a hydraulic fluid flow control valve, and a pre-set maximum force. Specimens were kept under constant stress for 3 minutes. The process was completed with a final cooling stage of 100° C while the specimens were still held under maximum compression stress.

Before and after treatment, weight and dimensions of the specimens were monitored. After the VTC process the specimens were dried in a convection oven (103° C) over-night, oven dry weight and dimensions were measured, and the oven dry density and moisture content after compression were determined. Equilibrium moisture content after conditioning in an environmentally-controlled room (20° C, 65% relative humidity) was calculated based on the oven dry mass after densification.

Preparation of CT Specimens

One non-compressed reference sample and one compressed sample of each of the two wood species were selected as specimens for CT. To achieve the maximum resolution the specimen

must have a transmission length as short as possible. Therefore they were shaped cylindrically with a diameter of approx. 2 mm, whereby the axis of these cylinders was chosen in longitudinal (not compressed) direction of the VTC samples (Figure 1). For the preparation of the CT specimens plies with rectangular cross sections in radial-tangential plane were cut from the reference samples and from the VTC compressed samples. In the case of poplar the plies were chosen to be within one growth ring, as the growth ring width is broader than the final diameter of the cylindrical specimen. Due to the minor difference between earlywood and latewood, the further analysis did not distinguish between earlywood and latewood. For Douglas-fir the CT specimens included earlywood and latewood. The earlywood proportions were 43 % for the uncompressed CT specimen and 73 % for the compressed one. These differences in earlywood/latewood proportion did not influence the evaluation of the tomographic data because the image data from tomography were virtually cut to suitable subvolumes. Various other influences e.g. those caused by resin canals were avoided in the choice of the subvolumes. Before the tomography was started, the specimens were stored under standard climate conditions (20° C and 65 % relative humidity) until equilibrium moisture content was reached; then they were packed under vacuum in plastic bags in order to minimize environmental influences during storage.

Computed Tomography and Image Analysis, Granulometric and Porosity Analysis

Computed microtomography (μ CT) and image analysis were used to provide information on the microstructure of both the initial (reference) and the compressed state of the investigated wood species. Additionally, further image analysis methods derived from mathematical morphology (also known as “granulometry”) were used to obtain information on the porous structure of uncompressed and compressed specimens.

The samples were scanned at the Upper Austrian University of Applied Sciences, Wels, Austria, with a phoenix|x-ray nanotom® 180. The nanofocus x-ray tube with 180 kV and the detector with 2300 x 2300 pixels enable a resolution down to 0.4 μ m. The so-called area of interest of the cylindrical specimens was chosen as 2 x 2 x 1.8 mm³. In this study the achieved resolution was 1 μ m edge length per volumetric pixel (voxel) for x-ray CT of the single specimens. Parameters used on the x-ray tube were 60 kV and 410 μ A. For one scan 1700 projections were made, which leads to a scanning time of 266 minutes per specimen. Relative humidity in the tomograph was between 31 % and 42 %, the temperature was between 22 and 24°C. A qualitative comparison of the first and last projection showed no apparent strain of the sample due to shrinkage movements caused by the climate conditions in the tomography device during the scanning time.

The next step in image analysis included the reduction of noise using a median filter which assured the preservation of the edges. After that the virtual data were cut to subvolumes of various sizes for the granulometric analysis. In order to evaluate thoroughly the smallest possible subvolume, where a sufficient representativeness of the results in relation to the largest pore sizes is still given, a broad range of subvolumes was chosen: 75 x 75 x 1200 μ m (radial x tangential x longitudinal), followed in size by 150 x 150 x 1200 μ m, 300 x 300 x 1200 μ m³, 600 x 600 x 1200 μ m³, and finally by 900 x 900 x 1200 μ m³ (only for Douglas-fir). For Douglas-fir the granulometric analysis was done separately for earlywood and latewood. The different subvolumes were analyzed in order to discern the influence of the chosen subvolume size on the results of the granulometric analysis. Before starting the granulometric analysis using MATLAB®, the virtual subvolumes were transformed into binary images. The threshold value for creating binary images was calculated using the so-

called gray level histogram based on the so-called Otsu method (Otsu 1979). With a family of growing structuring elements of certain size the distribution of these structuring elements (as referred to as ‘pores’) within the wood microstructure can be derived. When evaluating the size of a pore in a certain position in the sample, the diameter of the largest spherical structural element is taken that fits completely into the pore volume. A detailed description of the algorithm is given elsewhere (Lux et al. 2006, Standfest et al. 2010).

However one drawback of this method is, that pores e.g. shaped as ellipsoids are not described by one structural element, but by several lined up in a row. Regularly shaped structuring elements (ball shaped) as they were used for the granulometric analysis for this paper, therefore, cannot detect all anatomical features of wood; greater emphasis was placed on the diameter of pores rather than the length in case of such longish pores. The pore size distribution and mean pore sizes can be used to study the structural changes due to densification.

The porosity of CT data was calculated by voxel counting; the sum of voxels belonging to the pore space in the binary image data was divided by the sum of voxels of the whole subvolume.

The porosity C of wood was calculated according to the equation

$$C = 100 - (100 * \zeta_{od} / \zeta_{cw}) (\%) \quad (1)$$

with ζ_{od} = oven dry density, and ζ_{cw} = density of the cell wall and 1.5 g/cm^3 assumed for the cell wall density of wood. These results were compared with the results of the porosity calculated by voxel counting

Results and Discussion

Characteristics of Compressed (Densified) Wood

A main focus in this study was the relation between achieved densification and the resulting wood morphology. The oven-dry density of the various wood species after densification and, hence, of the analyzed sub- μm -CT specimens was significantly influenced by the applied compression stress (Table 1). At the same stress level of 5.5 MPa, a higher oven-dry density resulted for hardwood (hybrid poplar) compared to softwood (Douglas-fir); this is despite the fact that the average initial density of the hybrid poplar specimen (0.37 g/cm^3) was lower than the Douglas-fir specimen (0.45 g/cm^3). This result is due to the different anatomical structures of hardwoods and softwoods, like the presence of vessels in hardwoods, while in softwoods the principal elements are tracheids. The lower compression modulus of the hybrid poplar, hence, resulted in higher compression deformation. The lignin content of 20 % in hybrid poplar (Balatinecz and Kretschmann 2001, Klasnja et al. 2003) is notably lower than in Douglas-fir, which was determined to be around 32 % (Dadswell and Hawley 1929, Winandy and Morrell 1993). Softening of lignin largely dominates the effect of temperature and moisture on the time-dependent mechanical behavior of wood (Kärenlampi et al. 2003); furthermore the lower lignin content of hardwood compared to softwood also facilitates compression deformation. This is underlined by the additional fact that the hybrid poplar used in this study was obtained from 11-year-old fast-grown trees. The rapid growth created tension wood throughout the stem, which was confirmed by microscopic observation (Kutnar and Kamke 2010). The especially low lignin content and longer and thinner fibers in tension wood result in lower compression strength (Fang et al. 2008). In the G-layer the matrix is almost devoid of lignin, and the microfibrils are oriented nearly parallel to the fiber axis

(Clair 2010). The microfibril angle (MFA) is close to 0° in tension wood, which is significantly lower than MFA of Douglas-fir. Barnett and Bonham (2004) reported MFA variations of Douglas-fir to be 10° to 27°.

Comparison of the Initial and Compressed State

The morphology of wood significantly changes during the densification in the VTC process; this is mainly achieved by a reduction of the cell lumen volume.

Hybrid Poplar

Hybrid poplar (Figure 2) is a diffuse porous hardwood with minor differences in density between earlywood and latewood. The anatomic characteristics of the undensified hybrid poplar (e.g. homogeneous ray type, simple perforation plates, thin walled vessels solitary or radially joined in groups of two, three, or more, and libriform fibers), as analyzed by CT in the work described here (Figure 2a-c), coincide with previous results for poplar (Jourez et al. 2001). The morphology of densified poplar can be seen in Figure 2d, e, and f. The high strain in the VTC process drastically reduces the volume of void spaces in the specimens and deforms the cell lumens. This, however, happens without fracture of the cell walls. Vessels collapse and flatten in the direction of the compression, while the rays appear to buckle. Since the structural differences between earlywood and latewood in hybrid poplar are minor, differences in morphology between them after the VTC process could not be distinguished.

Douglas Fir

Earlywood and latewood in Douglas-fir can be clearly distinguished (Figures 3a-c). Annual rings are distinctly delineated by a pronounced narrow band of dark latewood. The structure of Douglas-fir wood is mostly built of tracheids, characterized by fine, close bands of spiral thickening. It has very fine rays, not visible to the naked eye, and longitudinal and transverse resin canals; the latter ones are much smaller than longitudinal canals and surrounded by epithelial cells. Since earlywood cells in softwoods possess larger lumens and thinner cell walls, they experience greater deformation than latewood cells during densification. Due to the thicker cell walls in latewood and, hence, their lower compressibility, the latewood cells do not buckle and do not undergo large deformations (see Figure 3d). Furthermore, the porosity of earlywood is larger than the porosity of latewood. Rays appear in wavy patterns and zigzag shape (Figure 3d), findings which were also reported by Dogu et al. (2010) for densified Scotch pine.

Granulometric and Porosity Analysis

Hybrid Poplar

The initial total porosity of the uncompressed reference samples was 66 to 67 % with a very broad and even bimodal distribution of the pore sizes (Figure 4a). Therefore the mean pore sizes of 34 and 40 µm (Table 2) only partly reflect the true situation; nevertheless it is a suitable measure when comparing the structure of uncompressed and compressed samples. The distributions of the uncompressed sample based on two different subvolume sizes in Figure 4a show pores with low pore diameter (pore sizes 3 – approx. 33 µm, with the peak maximum at approx. 16 µm, libriform fibers) and pores with larger and quite large diameters (pore sizes in a broad range of 34 – 100 µm, vessels). The upper limit (100 µm) reflects the order of magnitude of the diameter of the vessels as shown in Figure 2a-c. The proportion of

pores with sizes up to 33 μm is 61 % as an average for the two reference samples in Figure 4a; the proportion of the larger pores, hence, is 39%.

By far the biggest portion of the pore sizes remaining after compression is concentrated in a narrow peak at pore sizes up to approx. 22 μm with the peak maximum for the various subvolumes in the compressed state at approx. 7 μm ; this still corresponds to the data for the mean pore sizes (8 and 9 μm) as given in Table 2. Only in one case (subvolume “300”) a small shoulder in the peak flank on the right side with a pore size of approx. 14 μm can be discerned. Due to the broad distribution of pore sizes above approx. 33 μm in the reference sample (without compression), an average number of the percentage loss in pore size is not reliable and meaningful. For the libriform fibers with the peak pore size of approx. 16 μm and the peak pore size after compression of approx. 7 μm the average loss of pore size would be more than 50 %. The mean pore size of the whole investigated subvolume and including vessels and libriform fibers is reduced by the factor 4 – 5; this means that the mean pore size after densification is only 20 – 25% of the original pore size of the uncompressed wood structure.

The analysis of the various subvolumes showed that the smaller subvolumes, the greater the irregularities in the pore size distributions became. This fact points to the assumption that with smaller subvolumes (in relation to the biggest pores detected) the representativeness of the pore size distribution in this selected subvolume for the whole material investigated suffers. Obviously in smaller subvolumes the distribution of pores with small and large diameters can differ to sufficiently large subvolumes. With a minimum size of the subvolume of 300 x 300 x 1200 μm , only small differences in the various curves in Figure 4a for the uncompressed and for the compressed samples, resp., are given; this confirms that the size of the subvolumes used in the granulometric analysis is of minor importance as long as the subvolumes are sufficiently larger than the greatest pores. For the analysis reported here, this lowest acceptable ratio between the cross-sectional size of the subvolume and maximum pore size was defined with about 2.5. Contrary to the pore size distributions the calculated average values (porosity, mean pore size) showed less variation with small subvolumes (Table 2).

Figure 4b compares the absolute distributions of voxels according to the voxel count of the uncompressed reference sample and the compressed samples of the investigated hybrid poplar. This type of diagram offers the possibility to evaluate the total porosity as the area below the various distribution curves. The areas for the compressed samples, hence, are in the range of only a quarter to one third of the area of the uncompressed samples, reflecting the loss in porosity as summarized in Table 2.

The distribution of the voxels for the reference sample is, again, very broad and shows bimodal appearance. The threshold between the two parts of the bimodal distribution is at approx. 33 μm , as also shown in Figure 4a. The irregularities in the reference curve above 33 μm are accidental; an assignment of the various relative peak maxima to individual anatomical features is not possible. In the case of the VTC compression of the wood structure, the whole pore size distribution is concentrated more or less in one rather narrow peak with the peak maximum at approx. 7 μm . As already outlined above, the evaluated size of the pores rather reflects the diameter of the cross section of the pores at various positions than the full volume; this is especially true for pores with non-spherical shape. When evaluating the size of a pore, the largest diameter of a spherical structuring element fitting into the pore at any position is taken as measure. Pores with non-spherical shape (like with elliptic longitudinal cross section), hence, might be represented by several structuring elements lined up in a certain sequence. Nevertheless, the cross section diameters of such a stretched pore shape are determined correctly. Structuring elements with a certain shape, like

lines or rods can help in a further examination of ellipsoid shaped or even irregularly shaped pores. The total porosity of the selected subvolume, however, is not affected by this finding.

Douglas Fir

Different subvolumes of Douglas-fir earlywood and latewood were analyzed using the so-called granulometric method in order to evaluate the pore size distribution and mean pore sizes.

Uncompressed subvolumes within earlywood with a size between $75 \times 75 \times 1200 \mu\text{m}^3$ ("Reference 75") and $600 \times 600 \times 1200 \mu\text{m}^3$ ("Reference 600") show a total porosity of 76 % with a mean pore size of 31 - 33 μm (Table 3). The compressed subvolumes in earlywood had a total porosity of 32 to 35 %, which is less than half of the uncompressed subvolumes. The mean pore size was reduced to nearly one quarter compared to the original samples. The size of the subvolumes selected for the granulometric analysis had no influence on the determined total porosity and on the mean pore size.

For latewood the mean pore size and the porosity were significantly lower than for earlywood and similar to compressed earlywood (Table 3);

considering the possible accuracy in determining and calculating porosity and mean pore sizes as average values out of the determined pore size distribution no change in porosity and mean pore size was given for latewood before and after densification. For the uncompressed samples an even lower porosity and a slightly lower pore size than for the compressed samples was calculated (Table 3). The explanation of this might be found in sampling and is rather accidental.

The coefficient of variation of the pore size (see Table 3) in the compressed subvolumes of earlywood increased, whereas for latewood these values were similar for both, uncompressed and compressed samples.

The resulting pore size distributions of Douglas-fir earlywood are presented in Figure 5a. The uncompressed samples show broad distributions of the pore sizes from very small pores up to around 81 μm in diameter, as evaluated by granulometry. The peak value of 37 μm for the uncompressed state differs slightly from the mean pore size of 31 and 32 μm in Table 3. The absence of coincidence in the mean values of pore sizes and the location of the peak values when plotting their frequency indicate a non-symmetrical or even irregularly shaped pore size distribution, as it can be seen in Figure 4a for hybrid poplar and partly in Figure 5a for Douglas-fir earlywood. Similar to Figure 4 again in Figure 5 only the pore size distributions based on the larger subvolumes evaluated are shown.

The compressed earlywood subvolumes exhibit a very narrow pore size distribution (Figure 5a), showing the significant reduction in the pore sizes during the VTC process. More or less all voids of the tracheids with main diameters of 30 – 50 μm in their original shape before compression disappear; the relative proportion of small sized pores increases accordingly.

The curves representing the two untreated subvolumes also show a small but clear second maximum at a pore size of approximately 9 μm . This pore size corresponds presumably to the size of the pit chamber. The margo within the pits, however, cannot be detected by CT with the resolution given in this investigation. The proportion of these pores is approximately 9 %, based on the whole pore volume.

The distribution of the absolute number of pore voxels for Douglas-fir earlywood (Figure 5b) again shows the reduction in the pore sizes; additionally the area below the two curves (total number of pore voxels) as measure for the total pore volume is reduced significantly to 43 %

of the reference value; the same reduction can be calculated from Table 3 for the total porosity.

Also in Figure 5b, the small side peak of the reference sample at approx. 9 - 11 μm pore size (peak maximum at 10 μm) is visible, comprising approx. 9 % of the total area below the distribution curve. The main part of the pore size distribution for the reference sample in Figure 5 is given for the pore sizes between 15 and 57 μm ; a tiny peak (with only less than 0.2 % of the total number of voxels) is discernable for pore sizes of 75 – 83 μm . The irregularities in the centre part of the reference distribution at 31 μm , 39 μm , and 47 μm appear to be rather accidental.

For the distribution curve of the compressed earlywood sample the vast majority of the voxels is combined in the one narrow peak in the range of 3 – 22 μm ; a very small peak exists at 22 – 27 μm but comprises a proportion of only 0.6 % of the total voxel count.

The samples of Douglas-fir latewood show narrow pore size distributions even in the uncompressed state; nearly all material is concentrated in the low pore size region in the range of a pore diameter up to approx. 21 μm (Figure 6a). This is caused by the much smaller cell lumens in latewood (Figure 3). Due to the high compression modulus of its thick cell walls the compression of Douglas-fir latewood, hence, is quite low compared to earlywood. This is also visible in Figure 6a and 6b in which the various pore size distributions for the reference samples and the compressed samples are compared.

Figure 6b shows the distributions of voxel counts for the reference sample and the compressed sample, reflecting the porosity of the material as the area below the curves.

The graphs in Figure 5 and 6 again only comprehend the curves for the larger subvolumes. The smaller the selected subvolumes, the more the pore size distribution starts to show irregularities in its shape. This, especially, is the case for the larger pores in Douglas-fir earlywood. For this reason only the curves for the larger subvolumes are depicted in Figure 5 and 6. A general minimum ratio between the size of the subvolumes and the size of the largest pores is difficult to define. This depends on the uniformity of the pore size distribution as well as on the sample size in the CT measurements, the structure and composition of the material investigated, and the available calculation performance in the granulometric analysis. In this paper a ratio of around 2.5 has been estimated as best compromise between the various aspects.

With the density values for hybrid poplar of 0.394 g/cm^3 for the (uncompressed) reference and of 1.21 g/cm^3 for the compressed state the calculated porosity is 74 % and 19 %, resp. When evaluating the CT data, a porosity of 66 % to 67 % for the reference and 15 % to 23 % for the compressed state was concluded.

For Douglas-fir the two densities of 0.50 g/cm^3 for the uncompressed sample and 1.12 g/cm^3 for the compressed showed porosities of 67 % and 25 %; for these values. However, no distinction was made between earlywood and latewood. Based on the CT experiments 76 % for earlywood and 25 % to 26 % for latewood in the reference sample was determined. After compression the CT based porosity was 32 % to 35 % for earlywood and 29 % to 31 % for latewood. On a general basis the results based on the two methods correspond sufficiently well together.

Conclusions

The anatomical structures of Douglas-fir and hybrid poplar compressed in the so-called VTC process were analyzed using computed tomography and compared with the relevant wood

structures before densification. The pore size distribution and mean pore sizes describe the anatomical structure of both the original wood structure and the VTC densified wood. However, in the reference samples partly very broad or bimodal pore distributions occur, like in hybrid poplar and in Douglas fir earlywood; in such cases the mean pore sizes are of less significance.

Mainly earlywood (in Douglas-fir) and the vessels (in hybrid poplar) were affected by the compression, and their pore volumes decreased significantly. The porosity decreased to less than half of the original value for Douglas-fir earlywood and to approximately one quarter in hybrid poplar. The relevant mean pore sizes also decreased dramatically down to about one quarter.

Libriform fibers in hybrid poplar are less affected; the mean pore sizes of these smaller fibers were reduced by about 40 % by the VTC compression procedure.

For Douglas-fir latewood no apparent reduction of pores sizes could be determined by the VTC process; the original structure before compression remains more or less unchanged.

The study showed that CT is a suitable method for a nondestructive evaluation of densified wood on the microscopic level with low risk of preparation artifacts and with much easier preparation of the samples than is the case for any type of microscopy.

Since cellular features range in size from 1 – 100 μm , μCT with resolutions of very few microns is suitable for this micro-scale examination of wood and, consequently, will improve current knowledge concerning the morphology of wood. This might also be important when investigating the densified wood structure close to bond lines when jointing two wood surfaces.

As already outlined above, the detection of certain anatomical features in the wood structure, like the presence of narrow elongated pores, needs improved algorithms. Regularly shaped structuring elements (ball shaped), as were used for the granulometric analysis within this paper, rather reflects the diameter of such pores, but not their shape. This might be overcome using structuring elements of certain shape, like lines or rods when examining elongated or even irregularly shaped pores as they occur in the wood structure.

One of the main contributions of the CT method for the investigation of compressed wood is to distinguish the compression behavior of different parts of the wood structure, like earlywood and latewood; this could be shown evidently for Douglas-fir; contrary to this, for hybrid poplar more or less no discrimination between earlywood and latewood is given already in its uncompressed state. In Douglas-fir the compression is concentrated on the earlywood sections, whereas in hybrid poplar predominantly the vessels across the whole year ring are compressed. CT, therefore, is a valuable tool to follow the structural changes caused by the VTC process. In future different VTC process conditions and their consequences for the structure of the densified wood can be monitored and correlated. Furthermore, 3D reconstructions would enable developing a numerical model for explanation of deformations in wood during densification to be developed, the details of deformation at micro-scale could be predicted, and an insight into the relationship between microstructure and bulk properties of densified wood could be gained.

Acknowledgements

This project was gratefully supported by the 'FHplus in COIN' Programme of the Austrian

Research Promotion Agency (FFG) under project number 198353.

References

- Balatinecz JJ, Kretschmann DE (2001) Chapter 9: Properties and utilization of poplar wood. In: Poplar Culture in North America. Dickmann DI, Isebrands JG, Eckenwalder JE, Richardson J (eds). NRC Research Press, Ottawa
- Barnett JR, Bonham VA (2004) Cellulose microfibril angle in the cell wall of wood fibers. *Biol Rev* 79(2): 461–472
- Blomberg J, Persson B (2004) Plastic deformation in small clear pieces of Scots pine (*Pinus sylvestris*) during densification with the CaLignum process. *J Wood Sci* 50(4): 307–314
- Boonstra MJ, van Acker J, Kegel E, Stevens M (2007) Optimization of a two-stage heat treatment process: durability aspects. *Wood Sci Technol* 41(1): 31–57
- Clair B (2010) Maturation stress in developing tension wood. *Plant Physiology Preview. Am. Soc. Plant Biol.* 123(3): 1650-1658
- Dadswell HE, Hawley LF (1929) Chemical composition of wood in relation to physical characteristics. A preliminary study. *Ind Eng Chem* 21(10): 973–975
- Derome D, Griffa M, Koebel M, Carmeliet J (2011) Hysteretic swelling of wood at cellular scale probed by phase-contrast X-ray tomography. *J Struct Biol* 173(1): 180–190
- Dogu D, Tirak K, Candan Z, Unsal O (2010) Anatomical investigation of thermally compressed wood panels. *BioResources* 5(4): 2640–2663
- Dwianto W, Morooka T, Norimoto M, Kitajima T (1999) Stress Relaxation of Sugi (*Cryptomeria japonica* D. Don) Wood in Radial Compression under High Temperature Steam. *Holzforschung* 53(5): 541–546
- Epmeier H, Westin M, Rapp AO (2004) Differently Modified Wood: Comparison of some selected properties. *Scand J For Res* 19(5): 31–37
- Esteves B, Marques A, Domingos I, Pereira H (2007) Influence of steam heating on the properties of pine (*Pinus pinaster*) and eucalypt (*Eucalyptus globulus*) wood. *Wood Sci Technol* 41(3): 193–207
- Fang CH, Guibal D, Clair B, Gril J, Liu YM, Liu SQ (2008) Relationships between growth stress and wood properties in poplar I-69 (*Populus deltoides* Bartr.cv. “Lux” ex I-69/55). *Ann For Sci* 65(3): 307 (1-9)
- Grabner M, Salaberger D, Okochi T (2009) The Need of High Resolution μ -X-ray CT in Dendrochronology and in Wood Identification. In: ISPA 2009. 6th Int. Symp. Image and Signal Processing and Analysis. September 16 - 18, 2009 Salzburg, Austria; Proceedings, IEEE, 349–352
- Hillis WE (1984) High temperature and chemical effects on wood stability. Part 1: general considerations. *Wood Sci Technol* 18(4): 281–293
- Hsu WE, Schwald W, Schwald J, Shields JA (1988) Chemical and physical changes required for producing dimensionally stable wood-based composites. Part I: steam pretreatment. *Wood Sci Technol* 22 (3): 281–289
- Illman B, Dowd B (1999) High-resolution microtomography for density and spatial information about wood structures. In: Developments in X-ray tomography II. SPIE, Bellingham, Wash., 198–204
- Inoue M, Norimoto M, Tanahashi M, Rowell RM (1993) Steam or heat fixation of compressed wood. *Wood Fiber Sci.* 25(3): 224–235
- Jourez B, Riboux A, Leclercq A (2001) Anatomical characteristics of tension wood and opposite wood in young inclined stems of poplar (*Populus euramericana* cv ‘ghoy’). *IAWA Journal* 22(2): 133–157
- Kamke FA, Sizemore H (2008) Viscoelastic thermal compression of wood. USP 7,404,422
- Kärenlampi PP; Tynjälä P; Ström P (2003) Effect of temperature and compression on the mechanical behavior of steam-treated wood. *J Wood Sci* 49(4): 298–304
- Klasnja B, Kopitovic S, Orlovic S (2003) Variability of some wood properties of eastern cottonwood (*Populus deltoides* Bartr.) clones. *Wood Sci Technol* 37(3-4): 331–337

- Kollmann FP, Côté WA (1968) Principles of Wood Science and Technology. I. Solid Wood. Springer-Verlag Berlin. Heidelberg.
- Koch G, Puls J, Bauch J (2003) Topochemical characterisation of phenolic extractives in discoloured beechwood (*Fagus sylvatica* L.). *Holzforschung* 57(4): 339–345
- Kultikova EV (1999) Structure and Properties Relationships of Densified Wood. M.S. Thesis, Wood Science and Forest Products, Virginia Polytechnic Institute and State University, USA.
- Kutnar A, Kamke FA, Sernek M (2008) The mechanical properties of densified VTC wood relevant for structural composites. *Holz Roh Werkst* 66(6): 439–446
- Kutnar A, Kamke FA, Sernek M (2009) Density profile and morphology of viscoelastic thermal compressed wood. *Wood Sci Technol* 43(1): 57–68
- Kutnar A, Kamke AF (2010) Compression of wood under saturated steam, superheated steam and transient conditions at 150°C, 160°C, and 170°C. *Wood Sci Technol* 46(1-3): 73-88
- Kutnar A, Humar M, Kamke FA, Sernek M (2011) Fungal decay of viscoelastic thermal compressed (VTC) wood. *Eur. J Wood Wood Prod* 69(2): 325-328
- Mannes D, Marone F, Lehmann E, Stampanoni M, Niemz P (2010) Application areas of synchrotron radiation tomographic microscopy for wood research. *Wood Sci Technol*. 44(1): 67–84
- Mayo SC, Evans R, Chen F, Lagerstrom R (2009) X-ray phase-contrast micro-tomography and image analysis of wood microstructure. *Journal of Physics: Conference Series* 186(1): 12105
- Mayo SC, Chen F, Evans R (2010) Micron-scale 3D imaging of wood and plant microstructure using high-resolution X-ray phase-contrast microtomography. *J Struct Biol* 171(2): 182–188
- Metsä-Kortelainen S, Antikainen T, Viitaniemi P (2006) The water absorption of sapwood and heartwood of Scots pine and Norway spruce heat-treated at 170°C, 190°C, 210°C and 230°C. *Holz Roh Werkst* 64(3): 192–197
- Modzel G, Kamke FA, De Carlo F (2011) Comparative analysis of a wood - adhesive bondline. *Wood Sci Technol* 45(1): 147–158
- Navi P, Girardet F (2000) Effects of thermo-hydro-mechanical treatment on the structure and properties of wood. *Holzforschung* 54(3): 287–293
- Okochi T, Hoshino Y, Fujii H, Mitsutani T (2007) Nondestructive tree-ring measurements for Japanese oak and Japanese beech using micro-focus X-ray computed tomography. *Dendrochronologia* 24(2-3): 155–164
- Otsu N (1979) A Threshold Selection Method from Gray-Level Histograms. *IEEE T Syst Man Cyb* 9(1): 62–66
- Pfriem A, Zauer M, Wagenführ A (2009) Alteration of the pore structure of spruce (*Picea abies* (L.) Karst.) and maple (*Acer pseudoplatanus* L.) due to thermal treatment as determined by helium pycnometry and mercury intrusion porosimetry. *Holzforschung* 63(1): 94–98
- Plötze M, Niemz P (2011) Porosity and pore size distribution of different wood types as determined by mercury intrusion porosimetry. *Eur J Wood Wood Prod* 69(4): 649–657
- Rowell RM (2006) Chemical Modification of wood: A Short Review. *Wood Material Sci Eng* 1(1): 29–33
- Scholz G, Zauer M, van den Bulcke J, van Loo D, Pfriem A, van Acker J, Militz H (2010) Investigation on wax-impregnated wood. Part 2: Study of void spaces filled with air by He pycnometry, Hg intrusion porosimetry, and 3D X-ray imaging. *Holzforschung* 64(5): 587–593
- Schneider A, Wagner L (1974) Bestimmung der Porengrößenverteilung in Holz mit dem Quecksilber-Porosimeter. *Eur J Wood Wood Prod* 32(6): 216–224
- Schneider A (1979) Beitrag zur Porositätsanalyse von Holz mit dem Quecksilber-Porosimeter. *Eur J Wood Wood Prod* 37(8): 295–302
- Schneider A (1982) Untersuchungen über die Porenstruktur von Holzspanplatten mit Hilfe der Quecksilber-Porosimetrie. *Holz Roh Werkst* 40(12): 415–420
- Schweitzer F, Niemz P (1991) Untersuchungen zum Einfluß ausgewählter Strukturparameter auf die Porosität von Spanplatten. *Holz Roh Werkst* 49(1): 27–29
- Seborg RM, Millet MA, Stamm AJ (1945) Heat-stabilized compressed wood (Staypak). *Mech Eng* 67: 25–31

Standfest G, Kranzer S, Petutschnigg A, Dunky M (2010) Determination of the Microstructure of an Adhesive-Bonded Medium Density Fiberboard (MDF) using 3D Sub-Micrometer Computer Tomography. *J Adhesion Sci Technol* 24(8): 1501–1514

Sundqvist B, Karlsson O, Westermark U (2006) Determination of formic-acid and acetic acid concentrations formed during hydrothermal treatment of birch wood and its relation to colour, strength and hardness. *Wood Sci Technol* 40(7): 549–561

Tjeerdsma BF, Boonastra M, Pizzi A, Tekely P, Militz H (1998) Characterization of thermally modified wood: molecular reasons for wood performance improvement. *Holz Roh Werkst.* 56(3): 149–153

Trtik P, Dual J, Keunecke D, Mannes D, Niemz P, Stähli P, Kaestner A, Groso A, Stampanoni M (2007) 3D imaging of microstructure of spruce wood. *J Struct Biol* 159(1): 46–55

Varga D, Van der Zee ME (2008) Influence of steaming on selected wood properties of four hardwood species. *Holz Roh Werkst* 66(1): 11–18

Winandy JE, Morrell JJ (1993) Relationship between incipient decay, strength, and chemical composition of Douglas-fir heartwood. *Wood Fiber Sci.*, 25(3): 278–288

Wolcott MP (1989) Modelling viscoelastic cellular materials for the pressing of wood composites. PhD Dissertation. Virginia Tech, Blacksburg, Virginia, 182 pp.

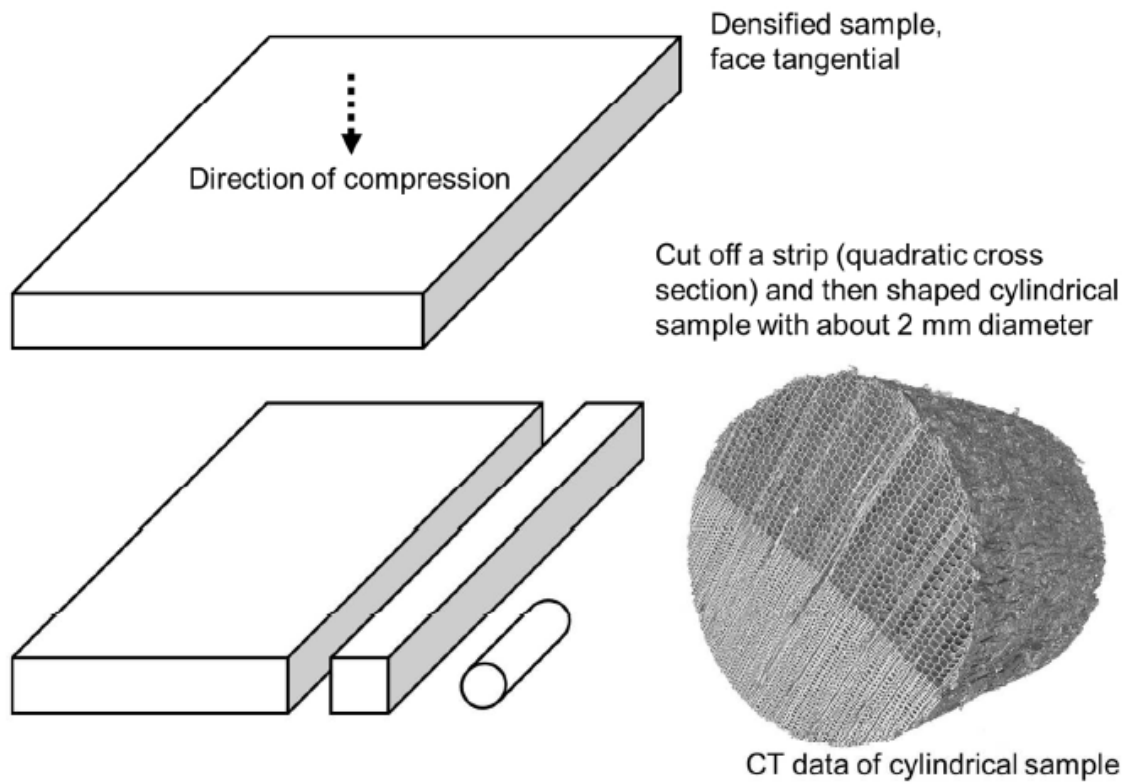


Figure 1. Scheme of the CT specimen preparation. Sizes are not to scale.

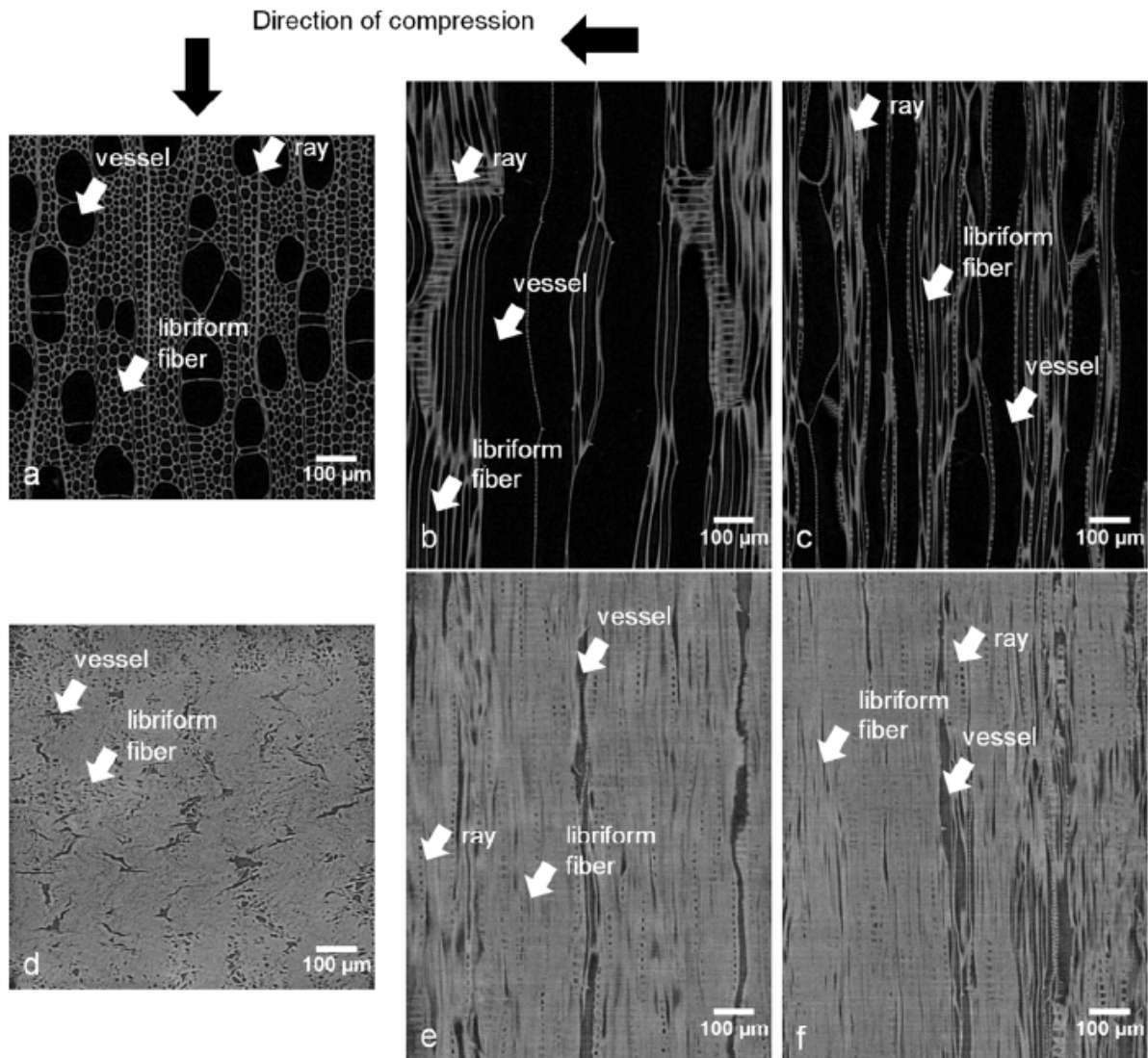


Figure 2. CT images of the different anatomical planes of hybrid poplar. a) uncompressed longitudinal cross section b) uncompressed radial section c) uncompressed tangential section d) with 5.5 MPa compressed longitudinal cross section e) with 5.5 MPa compressed radial section f) with 5.5 MPa compressed tangential section. Compression was performed in radial direction.

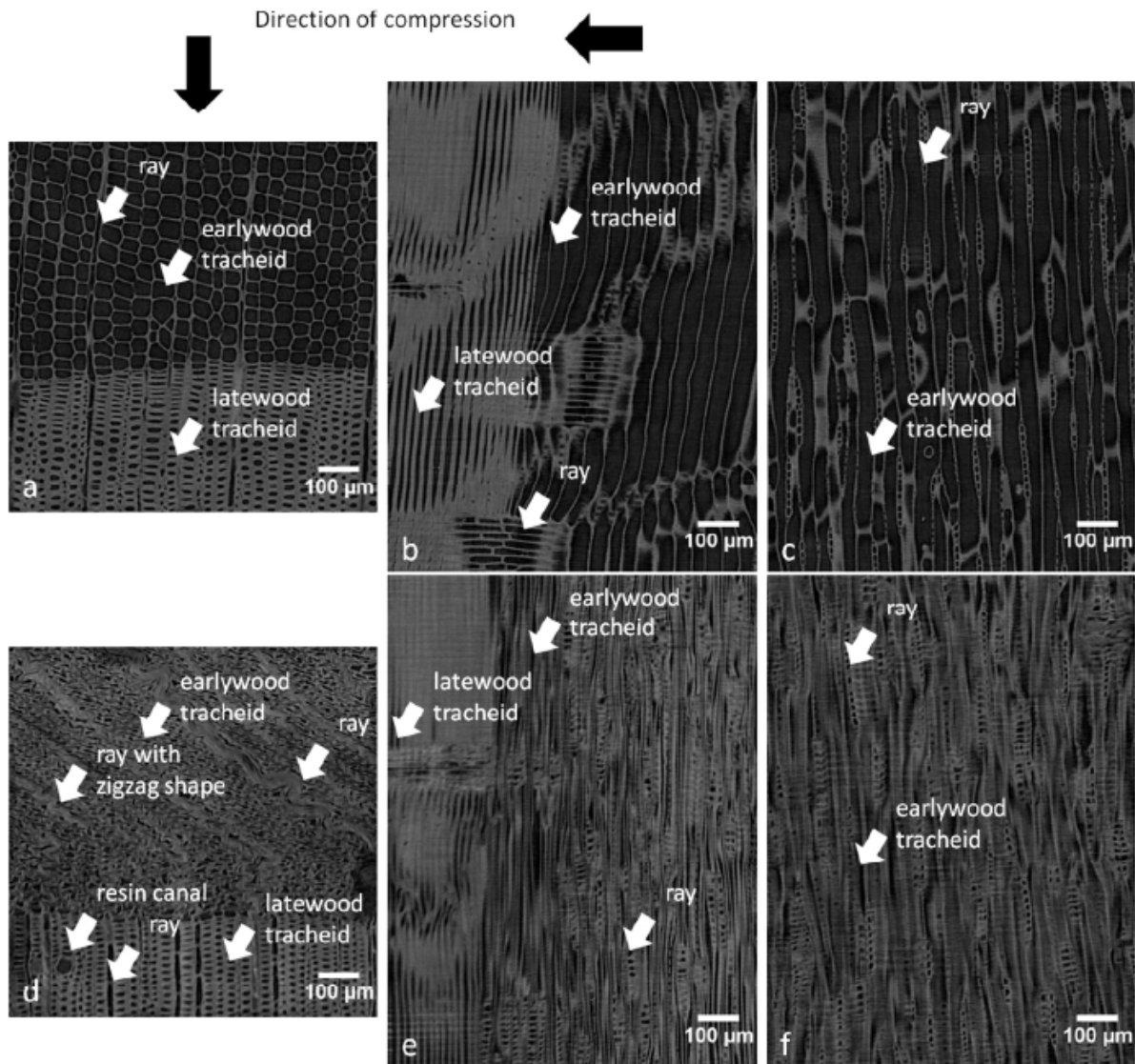


Figure 3. CT images of the different anatomical planes of Douglas fir. a) uncompressed longitudinal cross section b) uncompressed radial section c) uncompressed tangential section d) with 5.5 MPa compressed longitudinal cross section e) with 5.5 MPa compressed radial section f) with 5.5 MPa compressed tangential section. Compression was performed in radial direction.

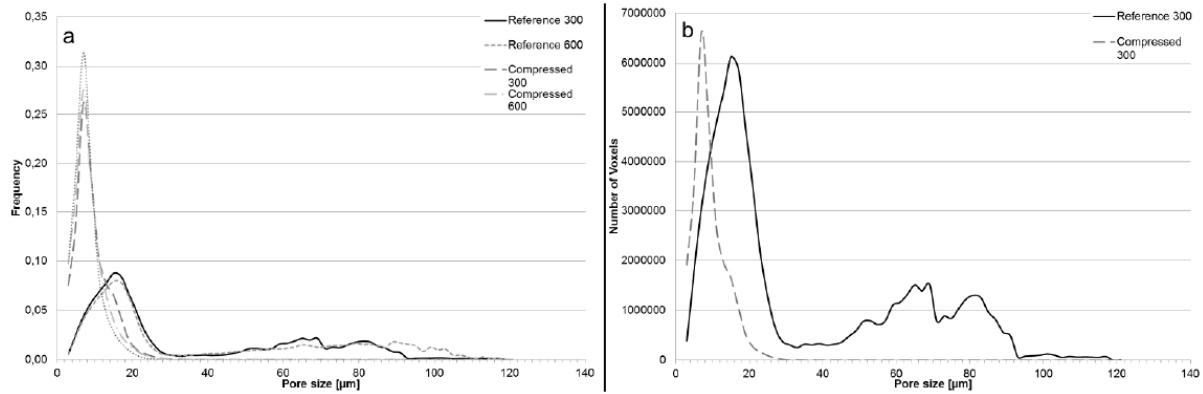


Figure 4. Pore size distributions of uncompressed (Reference) and VTC compressed hybrid poplar, as obtained by granulometric analysis after CT measurements. Data for individual pore sizes are shown in steps of 2 μm . Reference: uncompressed wood structure. Compressed: according to VTC process. The numbers indicate the size of the evaluated subvolumes (radial x tangential x longitudinal): 300: 300 x 300 x 1200 μm^3 ; 600: 600 x 600 x 1200 μm^3 . a) Frequency of pore sizes. b) Distribution of the number of pore voxels per individual pore size.

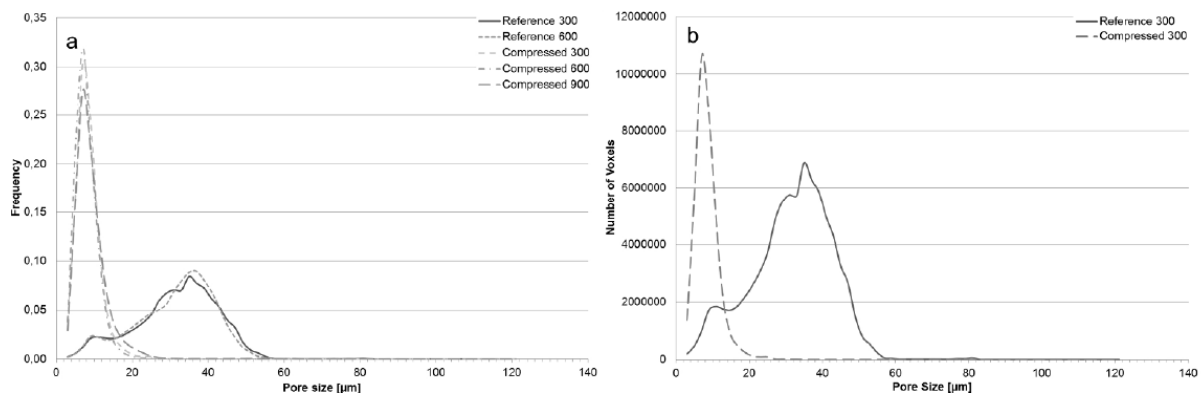


Figure 5. Pore size distribution obtained by granulometric analysis of Douglas-fir earlywood. Data for individual pore sizes are shown in steps of 2 μm . Reference: uncompressed wood structure. Compressed: according to VTC process. Reference: untreated wood structure. Compressed: according to VTC process. The numbers indicate the size of the evaluated subvolumes (radial x tangential x longitudinal): 300: 300 x 300 x 1200 μm^3 ; 600: 600 x 600 x 1200 μm^3 ; 900: 900 x 900 x 1200 μm^3 . a) Frequency of pore sizes. b) Distribution of the number of pore voxels per individual pore size.

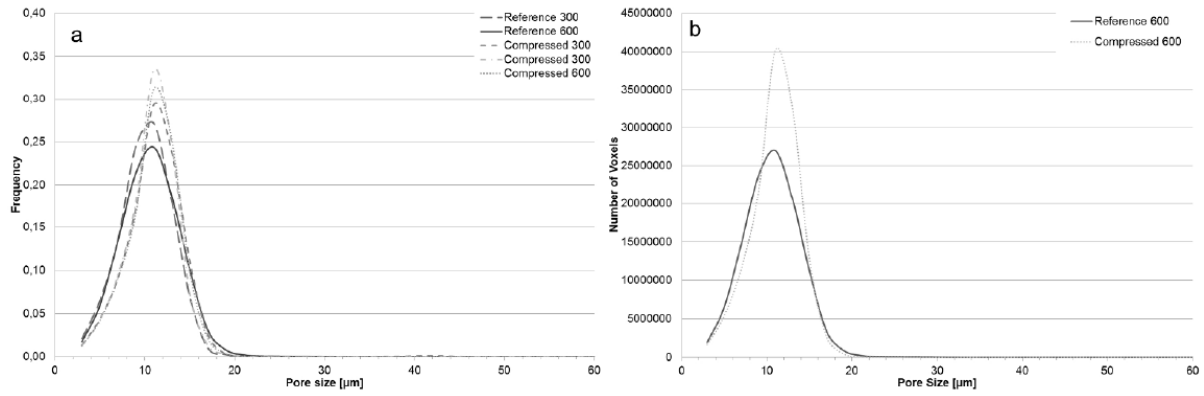


Figure 6. Pore size distribution obtained by granulometric analysis of Douglas-fir latewood. Data for individual pore sizes are shown in steps of 2 μm. Reference: uncompressed wood structure. Compressed: according to VTC process. Reference: wood structure without compression. Compressed: according to VTC process. The numbers indicate the size of the evaluated subvolumes (radial x tangential x longitudinal): 300: 300 x 300 x 1200 μm³; 600: 600 x 1200 μm³. a) Frequency of pore sizes. b) Distribution of the number of pore voxels per individual pore size.

Table 1. Oven-dry density of specimens before and after VTC compression at 170° C.

Stress level [MPa]	Wood species	Initial oven-dry density [g/cm ³]	Compressed oven-dry density [g/cm ³]
5.5	Douglas fir	0.498	1.12
5.5	Hybrid poplar	0.394	1.21

Table 2. Total porosity, mean pore size (MPS), standard deviation of the mean pore size (SD of MPS) and coefficient of variation (V) of the investigated subvolumes of hybrid poplar. Reference: untreated wood structure Compressed: according to VTC process. The numbers indicate the size of the evaluated subvolumes (radial x tangential x longitudinal): 75: 75 x 75 x 1200 μm³; 150: 150 x 150 x 1200 μm³; 300: 300 x 300 x 1200 μm³; 600: 600 x 600 x 1200 μm³; 900: 900 x 900 x 1200 μm³.

	Total Porosity [%]	Mean Pore Size [μm]	SD of MPS [μm]	V [%]
Reference 75	71	37 *	28 *	75 *
Reference 150	61	38 *	24 *	64 *
Reference 300	66	34 *	28 *	81 *
Reference 600	67	40 *	52 *	128 *
Compressed 75	24	8	3	41
Compressed 150	25	9	4	43
Compressed 300	23	9	3	47
Compressed 600 **	17	9	3	48
Compressed 600 **	15	8	3	44

*) Due to the broad and even bimodal distribution as shown in Figure 4 both mean pore size, standard deviation and coefficient of variation are rather mathematical results.

***) For “Compressed 600” two independent subvolumes of the same size were analyzed.

Table 3. Total porosity, mean pore size (MPS), standard deviation of the mean pore size (SD of MPS) and coefficient of variation (V) of the investigated subvolumes of earlywood and latewood of Douglas-fir. Reference: untreated wood structure. Compressed: according to VTC process. The numbers indicate the size of the evaluated subvolumes (radial x tangential x longitudinal): 75: 75 x 75 x 1200 μm^3 ; 150: 150 x 150 x 1200 μm^3 ; 300: 300 x 300 x 1200 μm^3 ; 600: 600 x 600 x 1200 μm^3 ; 900: 900 x 900 x 1200 μm^3 .

	Total Porosity [%]	Mean Pore Size [μm]	SD of MPS [μm]	V [%]
Earlywood				
Reference 75	76	33	12	37
Reference 150	76	32	11	35
Reference 300 35	76	32	11	34
Reference 600	76	31	10	33
Compressed 75 8	34	8	3	33
Compressed 150	32	8	3	32
Compressed 300	32	8	5	39
Compressed 600	32	8	5	37
Compressed 900	35	10	5	65
Latewood				
Reference 75	25	10	3	29
Reference 150	25	11	3	32
Reference 300	25	10	3	29
Reference 600	26	11	3	31
Compressed 75	29	12	3	27
Compressed 150	31	11	3	30
Compressed 300*	31	11	4	33
Compressed 300*	29	11	3	25
Compressed 600	30	11	3	26

*) For “Compressed 300” two independent subvolumes of the same size were analyzed.